

Suitability of available interatomic potentials for Sn to model its 2D allotropes

Marcin Maździarz^{a)}

*Institute of Fundamental Technological Research Polish Academy of Sciences,
Pawińskiego 5B, 02-106 Warsaw, Poland*

(Dated: 24 June 2024)

The suitability of a range of interatomic potentials for elemental tin was evaluated in order to identify an appropriate potential for modeling the stanene (2D tin) allotropes. Structural and mechanical properties of the flat (F), low-buckled (LB), high-buckled (HB), full dumbbell (FD), trigonal dumbbell (TD), honeycomb dumbbell (HD) and large honeycomb dumbbell (LHD) monolayer tin (stanene) phases, were gained by means of the density functional theory (DFT) and molecular statics (MS) calculations with ten different Tersoff, modified embedded atom method (MEAM) and machine-learning-based (ML-IAP) interatomic potentials. A systematic quantitative comparison and discussion of the results are reported.

Keywords: Tin; Stanene; 2D materials; Interatomic potentials; Force fields; DFT; Mechanical properties

I. INTRODUCTION

The scientific boom in 2D materials began in 2004 with the fabrication of graphene, a flat allotrope of carbon¹. Immediately, researchers became interested in other 2D materials as well, and naturally gravitated toward other elements in the carbon group of the 14th (formerly IV or IVA main) group of the periodic table, i.e. silicon (Si), germanium (Ge), tin (Sn), lead (Pb) and flerovium (Fl).

The flat, 2D form of tin (Sn, Latin: *stannum*) is called stanene and is a more analogue of the silicene (2D silicon), germanene (2D germanium) and plumbene (2D lead) than graphene (2D carbon). There is no layered form of tin analogous to graphite in nature. However, for Si, Ge, Sn, Pb, and Fl, it was possible to grow their 2D allotropes on suitable substrates by epitaxy^{2,3}.

Stanene is seen as a promising material for new electronic and spintronic applications due to its unique physical properties such as the quantum spin Hall (QSH) effect, topological superconductivity, giant magnetoresistance, perfect spin filter, and anomalous Seebeck effect⁴, and can potentially be used in electronics, optoelectronics, spintronics, thermotics, chemistry, mechanics, and sensor nanosystems⁵.

A total of approximately ten hypothetical polymorphs have been proposed in the scientific literature for 2D silicon, germanium, and tin⁶⁻⁸. If we limit ourselves to monolayers, this number decreases. Using *ab initio* calculations, it was possible here to relax and then analyze seven phases of stanene, namely flat (F), low-buckled (LB), high-buckled (HB), full dumbbell (FD), trigonal dumbbell (TD), honeycomb dumbbell (HD) and large honeycomb dumbbell (LHD). Complete structural and especially mechanical data for different stanene allotropes are very limited, see⁹⁻¹⁴.

If we could then all simulations in material modeling would be *ab initio* for sure, unfortunately their cost does not allow it and we use simplified methods like molecular dynamics/statics. A critical point in such calculations is the quality/universality/transferability of the interatomic potentials, i.e. how they behave outside the training set¹⁵⁻¹⁷.

Most interatomic potentials, both classical and machine learning-based (ML-IAP), are parameterized for 3D structures. The question naturally arises whether they are suitable

^{a)}Electronic mail: mmazdz@ippt.pan.pl.

for modeling their 2D allotropes. In the present research study, using *ab initio* calculations, we determined the structural and mechanical properties of seven 2D phases of Sn and then investigated whether the available potentials are able to reproduce these properties.

As far as I know, there is no publication that examines the ability of interatomic potentials for tin to describe its two-dimensional allotropes. Furthermore, there is no publication that comprehensively studies the structural and mechanical properties of stanene allotropes using DFT calculations. The objective of this paper is twofold: firstly, to determine the structural and mechanical properties of two-dimensional tin allotropes using *ab initio* methods, and secondly, to examine the ability of available interatomic potentials to reproduce these properties.

II. METHODOLOGY

The initial stage of the study involved the generation, based on the available literature^{6–8}, unit cells of hypothetical allotropes of monolayer tin. Seven such phases were successfully obtained. Then, using *ab initio* computations outlined in the Section II A, structural and mechanical data for these phases were determined and analyzed. These data contain lattice parameters, average cohesion energy, average bond length, average height, and 2D elastic constants. The data thus determined were then taken as reference results and marked as $\text{Value}^{\text{DFT}}$. The same data were then computed by classical molecular statics (MS), as outlined in the Section II A, and the ten interatomic potentials enumerated in Subsection II B. These results were then marked as $\text{Value}^{\text{potential}}$. Having reference data and those from the MS calculations, we specify the mean absolute percentage error (MAPE):

$$\text{MAPE} = \frac{100\%}{n} \sum_{t=1}^n \left| \frac{\text{Value}^{\text{DFT}} - \text{Value}^{\text{potential}}}{\text{Value}^{\text{DFT}}} \right|, \quad (1)$$

which allows us to quantify the analyzed interatomic potentials.

Furthermore, a series of classical molecular dynamics (MD) simulations (200 atoms and 10000 time steps, NVE-microcanonical ensemble) and the built-in LAMMPS function *timesteps/s* were employed to assess the computational cost of the examined interatomic potentials. The results were then normalized against the longest simulation time. For the purposes of performance testing, a serial version of LAMMPS and a laptop equipped with an Intel Core i5-8265U processor and Linux were used. LAMMPS (Stable Release from 2 August 2023) was compiled with the GCC compiler version 11.4.

A. Ab Initio and Atomistic Computations

The *ab initio* (relaxation of the structures, computation of cohesive energies and 2D elastic constants) and atomistic (relaxation of the structures, computation of cohesive energies and 2D elastic constants, CPU cost of the analyzed potentials) methodology here is analogous to that in⁷. The programs used are: for density functional theory (DFT)^{18,19} and density functional perturbation theory (DFPT)²⁰ ABINIT²¹ with generalized gradient approximation (GGA), PBEsol²² as exchange-correlation (XC) functional and optimized norm-conserving Vanderbilt pseudopotential²³ (ONCVPP) taken from PseudoDojo project²⁴. For molecular statics (MS) and molecular dynamics (MD), the Large-scale Atomic/Molecular Massively Parallel Simulator (LAMMPS)²⁵ and for visualization and analysis, the Open Visualization Tool (OVITO)²⁶.

B. Interatomic Potentials

The parametrizations of the potentials enumerated hereafter were obtained from the NIST Interatomic Potentials Repository²⁷ and/or from LAMMPS code sources and/or through

the assistance of the authors of the aforementioned publications.

1. Tersoff2016²⁸: the Tersoff potential parameters fitted to an *ab-initio* derived training set that included the equation of state, cohesive energy, lattice constants, buckling height, in-plane stiffness and phonon dispersion of low-buckled stanene, calculated using density functional theory (DFT)
2. MEAM1997²⁹: the modified embedded atom method (MEAM) potential fitted to cohesive energy, lattice and elastic constant of α and β tin
3. MEAM2017³⁰: the modified embedded atom method (MEAM) potential fitted to both solid and liquid properties of tin
4. MEAM2018a³¹: the modified embedded atom method (MEAM) potential fitted to high temperature elastic constants of tin
5. MEAM2018b³²: the modified embedded atom method (MEAM) potential's parameters were optimized based on the force-matching method using the density functional theory (DFT) database of energies and forces of atomic configurations under different conditions
6. RANN³³: combination of the embedded atom method (EAM) and rapid artificial neural network potential fitted to the *ab-initio* derived energies and forces of the four different solid phases of Sn
7. DP-PBE³⁴: the machine-learning-based (ML-DP-PBE) potential (DeePMD³⁵) obtained by training on the *ab initio* data from density functional theory calculations using the PBE³⁶ exchange–correlation functional
8. DP-SCAN³⁴: the machine-learning-based (ML-DP-SCAN) potential (DeePMD³⁵) obtained by training on the *ab initio* data from density functional theory calculations using the SCAN³⁷ exchange–correlation functional
9. POLY³⁸: the polynomial machine-learning potential for elemental and alloy systems obtained by training on a datasets generated from density functional theory calculations for prototype structures
10. MTP³⁹: the moment tensor machine-learning interatomic potential (MTP)⁴⁰ obtained by training on the *ab initio* data from density functional theory calculations for reference configurations

III. RESULTS

Following the generation of 2D-Sn unit cells, the subsequent step was to relax and optimize these structures through *ab initio* calculations. The resulting unit cells for the seven stanene allotropes, i.e, the flat (F):(*hP*2, P6/mmm, No.191), low-buckled (LB):(*hP*2, P $\bar{3}$ m1, No.164), high-buckled (HB):(*hP*2, P $\bar{3}$ m1, No.164), full dumbbell (FD):(*hP*3, P $\bar{6}$ m2, No.187), trigonal dumbbell (TD):(*hP*7, P $\bar{6}$ 2m, No.189), honeycomb dumbbell (HD):(*hP*8, P $\bar{6}$ 2m, No.189) and large honeycomb dumbbell (LHD):(*hP*10, P6/mmm, No.191) are depicted in Figs. 1a)-g) and the additional crystallographic data for them are stored in the Crystallographic Information Files (CIFs) in the Supplementary material V. All the stanene polymorphs analyzed here, as well as silicene and germanene^{7,8}, have 2D hexagonal symmetry, which should imply planar isotropy of physical properties.

The structural and mechanical properties of the seven stanene polymorphs, obtained as a result of *ab initio* calculations, are presented in Table I. These include lattice parameters, average cohesive energy, average bond length, average height, 2D elastic constants, 2D Young's modulus, Poisson's ratio, and 2D Kelvin moduli. It can be observed that the data available from other calculations for low-buckled and large honeycomb dumbbell stanene

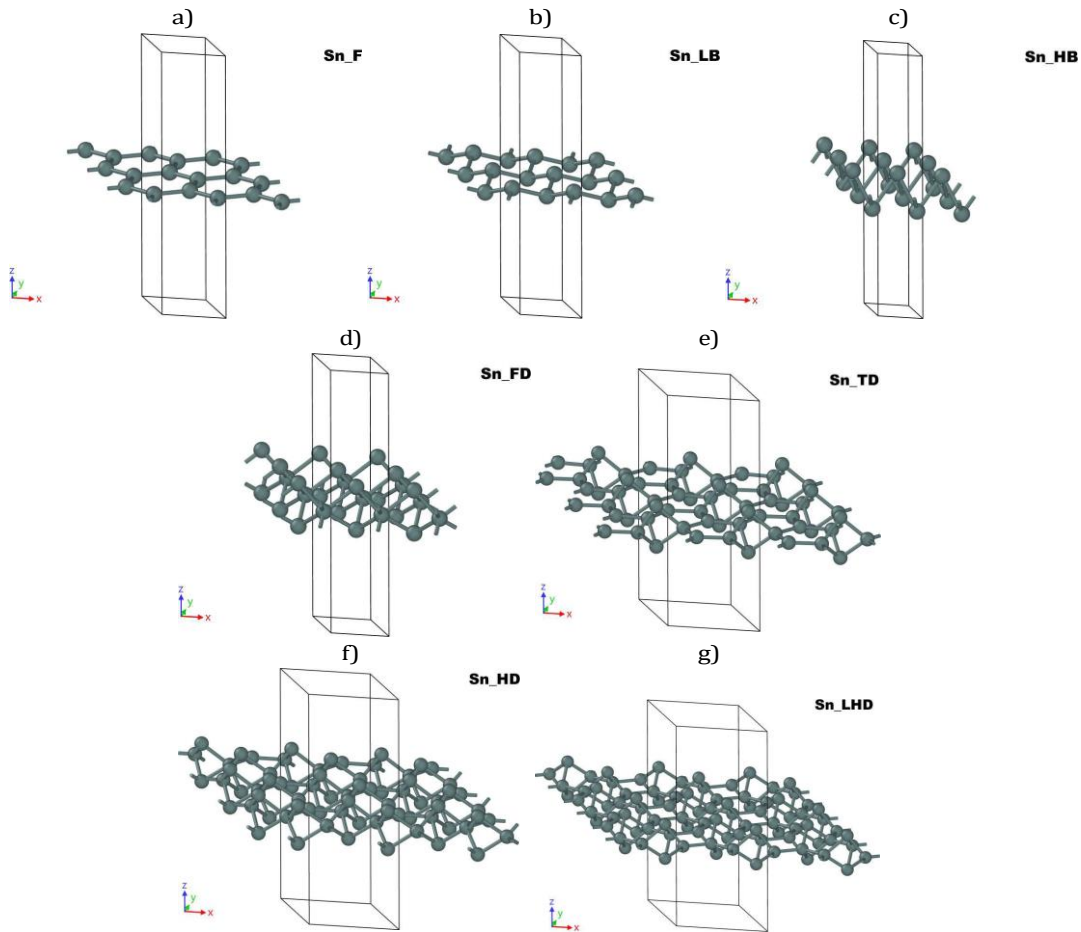


FIG. 1. Polymorphs of stanene: a) flat (F), b) low-buckled (LB), c) high-buckled (HB), d) full dumbbell (FD), e) trigonal dumbbell (TD), f) honeycomb dumbbell (HD), g) large honeycomb dumbbell (LHD).

polymorphs are in reasonable agreement with the current findings. As can be also observed, all calculated 2D Kelvin moduli for all seven phases are positive, indicating the mechanical stability of all the structures⁴¹.

The calculated with the use of molecular statics and the ten examined interatomic potentials for stanene (Terstoff, MEAM ($\times 4$) and machine-learning-based (ML-IAP ($\times 5$)), listed in Section II B, twelve structural and mechanical properties, i.e., lattice parameters a , b , average cohesive energy E_c , average bond length d , average height h , 2D elastic constants C_{ij} , 2D Kelvin moduli K_i of the flat stanene (F) phase are gathered in Table II, of the low-buckled (LB) stanene in Table III, of the high-buckled (HB) stanene in Table IV, of full dumbbell (FD) stanene in Table V, of the trigonal dumbbell stanene (TD) in Table VI, the honeycomb dumbbell (HD) in Table VII and of the large honeycomb dumbbell stanene (LHD) in Table VIII, respectively. The aforementioned results, for each of the seven stanene allotropes, were then compared with those from the DFT computations utilizing the mean absolute percentage error (MAPE), as defined in Eq. 1.

The cumulative score of all the potentials analyzed in terms of minimum total MAPE, see Table VIII, shows the MEAM2018b potential as the best, the MEAM2017 potential as the second, and the DP-PBE potential as the third. From the point of view of computational cost in terms of relative performance measured as normalized timesteps/second in molecular dynamics (MD) simulations, MEAM2018b wins, second is Terstoff2016 and

TABLE I. Structural and mechanical properties of flat (F), low-buckled (LB), high-buckled (HB), full dumbbell (FD), trigonal dumbbell (TD), honeycomb dumbbell (HD) and large honeycomb dumbbell (LHD) stanene phases from density functional theory (DFT) calculations: lattice parameters a, b (Å), average cohesive energy E_c (eV/atom), average bond length d (Å), average height h (Å), 2D elastic constants C_{ij} (N/m), 2D Young's modulus E (N/m), Poisson's ratio ν and 2D Kelvin moduli K_i (N/m).

Polymorph	F		LB		HB		FD		TD		HD		LHD	
Source	This work	Refs. This work	Refs.	This work	Refs. This work	This work	Refs. This work	This work	Refs. This work	This work	Refs. This work	This work	Refs. This work	
a	4.753	4.594	4.66 ^b , 4.67 ^c	3.329	3.413 ^d	4.309	7.821	7.646	7.74 ^c	8.890	9.05 ^c			
b	4.753	4.594	4.66 ^b , 4.67 ^c	3.329	3.413 ^d	4.309	7.821	7.646	7.74 ^c	8.890	9.05 ^c			
$-E_c$	2.719	2.844	2.68	3.179	3.043	2.933	3.040	2.84 ^c	3.062	2.86 ^c				
d	2.746 [†]	2.791	2.83 ^a , 2.83 ^b	3.266	3.012	2.830	2.945	2.897						
h	0.6	0.875	0.85, 0.9	2.497	3.267	3.514	3.290	3.34 ^c	3.404	3.42 ^c				
C_{11}	31.335	23.426	28.6 ^a	44.046	15.251	27.650	27.923	33.028						
C_{22}	31.335	23.426	28.6 ^a	44.046	15.251	27.650	27.923	33.028						
C_{12}	17.704	8.082	11.3 ^a	28.644	8.710	11.031	13.078	15.753						
C_{33}	6.815	7.672	8.65 ^a	7.701	3.270	8.310	7.422	8.637						
E	21.332	20.638	24.14 ^a , 24.46 ^b	25.417	10.276	23.250	21.797	25.514						
ν	0.565	0.345	0.395 ^a , 0.390 ^b	0.650	0.571	0.399	0.468	0.477						
K_I	49.039	31.508		72.690	23.961	38.681	41.001	48.782						
K_{II}	13.630	15.345		15.401	6.540	16.620	14.845	17.275						
K_{III}	13.630	15.345		15.401	6.540	16.620	14.845	17.275						

^a Ref. 14, ^b Ref. 13, ^c Ref. 6 ^d Ref. 10.

[†] An average bond lengths calculated using radial pair distribution function with a *cut-off* radius = 3.5 Å and a number of histogram bins = 1000²⁶.

third is MEAM2017, but the differences here are minimal. Classical potentials are up to 3 orders of magnitude faster than machine-learning-based ones. Let's also look at other aspects of the performance of the potentials. Only four potentials, namely Tersoff2016, MEAM1997, MEAM2018b and POLY correctly reproduce the symmetries of all 2D-Sn phases. All five machine-learning-based potentials fail to reproduce the required isotropy of the stiffness tensor for all stanene phases, see Table VIII, either/and exhibit a spurious lack of mechanical stability, see Table II. They appear to violate the principle of symmetry (*Neumann's Principle*)^{42,43}, which states that the symmetry elements of any physical property of a crystal must include the symmetry elements of the crystal's point group. Since the mathematical form of such potentials is unconstrained and does not result from physical approximations, they show difficulty in extrapolating to atomic structures/compositions that differ greatly from those in the data on which they were trained⁴⁴.

TABLE II. Structural and mechanical properties of flat (F) stanene from molecular calculations: lattice parameters a, b (Å), average cohesive energy E_c (eV/atom), average bond length d (Å), average height h (Å), 2D elastic constants C_{ij} (N/m), 2D Kelvin moduli K_i (N/m), mean absolute percentage error (MAPE) (%).

Method	DFT	Tersoff 2016	MEAM 1997	MEAM 2017	MEAM 2018a	MEAM 2018b	RANN 2023	DP-PBE 2023	DP-SCAN 2023	POLY 2023	MTP 2024
a	4.753	4.987	5.274	4.856	5.419	4.939	5.412 [†]	4.913	4.739	4.875	4.705
b	4.753	4.987	5.274	4.856	5.419	4.939	5.420 [†]	4.913	4.739	4.875	4.705
$-E_c$	2.719	3.191	2.249	2.489	2.119	2.656	2.548	3.075	2.235	2.614	2.553
d	2.746	2.879	3.047	2.805	3.092	2.851	3.126	2.837	2.735	2.816	2.718
h	0.0	0.0	0.0	0.0	0.0	0.0	0.0	0.0	0.0	0.0	0.0
C_{11}	31.335	40.547	25.890	28.729	24.984	27.073	9.707	11.347	165.106	32.077	49.430
C_{22}	31.335	40.547	25.890	28.729	24.984	27.073	8.723	11.347	165.106	32.077	49.430
C_{12}	17.704	16.209	17.699	10.960	16.023	19.754	10.765	13.528	180.506	30.118	23.780
C_{33}	6.815	12.169	4.095	8.884	4.481	3.660	-0.740	-1.091	-7.700	0.980	12.825
K_I	49.039	56.756	43.590	39.689	41.007	46.827	19.969	24.876	345.611	62.196	73.211
K_{II}	13.630	24.338	8.191	17.769	8.962	7.320	-1.539	-2.181	-15.400	1.959	25.650
K_{III}	13.630	24.338	8.191	17.769	8.962	7.320	-1.480	-2.181	-15.400	1.959	25.650
MAPE _F		31.881	19.616	16.347	21.081	17.831	56.425	51.960	275.991	33.644	42.981

[†] Potential does not reproduce the correct symmetry of the structure ($a \neq b$),

* Negative Kelvin moduli K_i indicating a lack of mechanical stability.

TABLE III. Structural and mechanical properties of low-buckled (LB) stanene from molecular calculations: lattice parameters a, b (Å), average cohesive energy E_c (eV/atom), average bond length d (Å), average height h (Å), 2D elastic constants C_{ij} (N/m), 2D Kelvin moduli K_i (N/m), mean absolute percentage error (MAPE) (%).

Method	DFT	Tersoff 2016	MEAM 1997	MEAM 2017	MEAM 2018a	MEAM 2018b	RANN 2023	DP-PBE 2023	DP-SCAN 2023	POLY 2023	MTP 2024
a	4.594	4.676	4.959	4.856 [†]	5.419 [†]	4.500	3.288 [‡]	3.358	4.431	4.731	4.304
b	4.594	4.676	4.959	4.856 [†]	5.419 [†]	4.500	3.288 [‡]	3.358	4.431	4.731	4.304
$-E_c$	2.844	3.311	2.293	2.489	2.119	2.743	2.900	3.613	2.492	2.651	2.760
d	2.791	2.875	3.019	2.805	3.092	2.823	3.326	3.322	2.924	2.851	2.777
h	0.875	0.992	0.956	0.000	0.000	1.104	2.831	2.612	1.415	0.814	1.240
C_{11}	23.426	12.678	12.978	28.729	24.984	11.730	48.115	23.558	90.351	22.791	16.961
C_{22}	23.426	12.678	12.978	28.729	24.984	11.730	48.115	23.558	90.351	22.791	16.961
C_{12}	8.082	3.134	2.502	10.960	16.023	3.110	28.561	18.093	38.954	16.590	2.235
C_{33}	7.672	4.772	5.238	8.884	4.481	4.310	9.777	2.732	25.699	3.100	7.393
K_I	31.508	15.812	15.480	39.689	41.007	14.840	76.675	41.651	129.305	39.381	19.196
K_{II}	15.345	9.544	10.476	17.769	8.962	8.619	19.554	5.465	51.398	6.201	14.725
K_{III}	15.345	9.544	10.476	17.769	8.962	8.619	19.554	5.465	51.398	6.201	14.725
MAPE _{LB}		29.385	29.752	23.219	36.560	31.725	82.619	54.066	171.221	28.022	19.708

[†] Input low-buckled (LB) structure converges to flat (F) one,

[‡] Input low-buckled (LB) structure converges to high-buckled (HB) one.

TABLE IV. Structural and mechanical properties of high-buckled (HB) stanene from molecular calculations: lattice parameters a, b (Å), average cohesive energy E_c (eV/atom), average bond length d (Å), average height h (Å), 2D elastic constants C_{ij} (N/m), 2D Kelvin moduli K_i (N/m), mean absolute percentage error (MAPE) (%).

Method	DFT	Tersoff 2016	MEAM 1997	MEAM 2017	MEAM 2018a	MEAM 2018b	RANN 2023	DP-PBE 2023	DP-SCAN 2023	POLY 2023	MTP 2024
a	3.329	3.043	3.428	3.300	3.480	3.232	3.288	3.358	3.317 [†]	3.297	3.151
b	3.329	3.043	3.428	3.300	3.480	3.232	3.288	3.358	3.332 [†]	3.297	3.151
$-E_c$	3.179	2.978	2.582	2.602	2.343	2.885	2.900	3.613	3.180	2.771	3.477
d	3.266	3.065	3.428	3.299	3.481	3.217	3.326	3.322	3.269	3.295	3.057
h	2.497	2.565	2.994	3.092	3.411	2.585	2.831	2.612	2.538	3.442	2.257
C_{11}	44.046	69.924	54.584	50.187	60.558	89.418	48.115	23.557	471.698	54.196	155.850
C_{22}	44.046	69.924	54.584	50.187	60.558	89.418	48.115	23.557	387.154	54.196	155.850
C_{12}	28.644	27.100	40.962	49.800	44.448	28.848	28.561	18.094	255.274	32.780	94.697
C_{33}	7.701	21.412	6.811	0.194	8.055	30.285	9.777	2.731	75.268	10.708	30.577
K_I	72.690	97.024	95.546	99.987	105.006	118.265	76.675	41.651	681.175	86.976	250.547
K_{II}	15.401	42.824	13.622	0.388	16.110	60.570	19.554	5.463	177.676	21.415	61.154
K_{III}	15.401	42.824	13.622	0.388	16.110	60.570	19.554	5.463	150.537	21.415	61.154
MAPE _{HB}		60.250	17.216	39.709	22.247	97.449	10.965	32.323	515.742	20.904	159.182

[†] Potential does not reproduce the correct symmetry of the structure ($a \neq b$).

TABLE V. Structural and mechanical properties of full dumbbell (FD) stanene from molecular calculations: lattice parameters a, b (\AA), average cohesive energy E_c (eV/atom), average bond length d (\AA), average height h (\AA), 2D elastic constants C_{ij} (N/m), 2D Kelvin moduli K_i (N/m), mean absolute percentage error (MAPE) (%).

Method	DFT	Tersoff 2016	MEAM 1997	MEAM 2017	MEAM 2018a	MEAM 2018b	RANN 2023	DP-PBE 2023	DP-SCAN 2023	POLY 2023	MTP 2024
a	4.309	3.056	3.427	3.306	3.459	4.359	3.299	3.343	3.358	3.229	4.617
b	4.309	3.056	3.427	3.306	3.459	4.359	3.299	3.343	3.358	3.229	4.617
$-E_c$	3.043	3.147	2.741	2.746	2.516	2.782	2.955	3.649	3.200	2.968	3.283
d	3.012	3.074	3.428	3.306	3.361	2.998	3.348	3.355	3.282	3.303	2.909
h	3.267	5.096	5.841	6.017	6.461	3.170	5.699	5.527	5.042	5.755	2.623
C_{11}	15.251	98.990	74.550	70.174	83.734	24.382	63.948	35.552	83.271	109.906 [‡]	34.089
C_{22}	15.251	98.990	74.550	70.174	83.734	24.382	63.948	35.552	83.271	109.906 [‡]	34.089
C_{12}	8.710	37.917	56.256	69.053	60.445	12.875	42.490	21.910	53.525	45.523 [‡]	6.230
C_{33}	3.270	30.536	9.147	0.561	11.645	5.754	10.729	6.821	14.873	35.318 [‡]	13.929
K_I	23.961	136.907	130.807	139.227	144.179	37.257	106.439	57.462	136.797	155.429	40.319
K_{II}	6.540	61.073	18.294	1.121	23.289	11.507	21.458	13.642	29.746	64.384	27.858
K_{III}	6.540	61.073	18.294	1.121	23.289	11.507	21.458	13.642	29.746	70.637	27.858
MAPE _{FD}		411.450	222.917	208.446	266.200	42.292	199.120	93.519	277.683	472.326	124.271

[‡] Potential does not reproduce the isotropy of the elasticity tensor ($2 \cdot C_{33} \neq C_{11} - C_{12}$).

TABLE VI. Structural and mechanical properties of trigonal dumbbell (TD) stanene from molecular calculations: lattice parameters a, b (\AA), average cohesive energy E_c (eV/atom), average bond length d (\AA), average height h (\AA), 2D elastic constants C_{ij} (N/m), 2D Kelvin moduli K_i (N/m), mean absolute percentage error (MAPE) (%).

Method	DFT	Tersoff 2016	MEAM 1997	MEAM 2017	MEAM 2018a	MEAM 2018b	RANN 2023	DP-PBE 2023	DP-SCAN 2023	POLY 2023	MTP 2024
a	7.821	8.102	8.249	7.869	8.181	7.951	7.130 [†]	7.781	7.678 [†]	8.302	8.428
b	7.821	8.102	8.249	7.869	8.181	7.951	6.414 [†]	7.781	7.806 [†]	8.302	8.428
$-E_c$	2.933	3.142	2.386	2.524	2.264	2.773	2.903	3.293	2.867	2.669	4.020
d	2.830	2.981	3.050	2.904	3.122	2.885	3.238	2.910	2.918	3.032	1.718
h	3.514	3.990	4.172	3.940	4.845	3.638	3.185	4.145	4.891	2.936	3.809
C_{11}	27.650	23.369	19.461	28.514	21.261	17.086	21.545	14.818	33.650	26.747 [‡]	32.672
C_{22}	27.650	23.369	19.461	28.514	21.261	17.086	27.134	14.818	52.417	26.747 [‡]	32.672
C_{12}	11.031	-0.219	8.511	11.929	9.824	8.357	8.056	13.058	24.280	24.511 [†]	20.993
C_{33}	8.310	11.794	5.475	8.292	5.719	4.365	8.288	0.880	3.980	2.985 [‡]	5.840
K_I	38.681	23.588	27.972	40.442	31.085	25.443	31.895	27.876	65.427	51.258	53.665
K_{II}	16.620	23.150	10.950	16.585	11.437	8.729	16.784	1.761	20.639	2.236	11.680
K_{III}	16.620	23.588	10.950	16.585	11.437	8.729	16.575	1.761	7.960	5.970	11.680
MAPE _{TD}		27.356	22.347	4.121	20.876	24.294	10.130	36.787	39.625	35.067	29.567

[†] Potential does not reproduce the correct symmetry of the structure ($a=b$),

[‡] Potential does not reproduce the isotropy of the elasticity tensor ($2 \cdot C_{33} \neq C_{11} - C_{12}$).

TABLE VII. Structural and mechanical properties of honeycomb dumbbell (HD) stanene from molecular calculations: lattice parameters a, b (\AA), average cohesive energy E_c (eV/atom), average bond length d (\AA), average height h (\AA), 2D elastic constants C_{ij} (N/m), 2D Kelvin moduli K_i (N/m), mean absolute percentage error (MAPE) (%).

Method	DFT	Tersoff 2016	MEAM 1997	MEAM 2017	MEAM 2018a	MEAM 2018b	RANN 2023	DP-PBE 2023	DP-SCAN 2023	POLY 2023	MTP 2024
a	7.646	7.683	7.769	7.524	7.023 [†]	7.730	8.007	9.741 [†]	8.659 [†]	7.435	7.953
b	7.646	7.683	7.769	7.524	7.021 [†]	7.730	8.007	4.782 [†]	7.380 [†]	7.435	7.953
$-E_c$	3.040	2.881	2.401	2.468	2.292	2.788	2.845	3.579	2.894	2.820	3.315
d	2.945	3.031	3.096	3.005	3.344	2.966	2.937	3.176	3.039	3.212	2.831
h	3.290	3.797	3.970	3.885	5.429	3.288	2.943	4.505	3.186	3.903	2.607
C_{11}	27.923	44.952	14.868	24.448	10.715	17.803	36.010	19.795	41.728	15.973 [‡]	36.693
C_{22}	27.923	44.952	14.868	24.448	10.729	17.803	36.010	14.854	2.145	18.338 [‡]	36.693
C_{12}	13.078	4.265	10.089	10.562	10.949	7.318	8.930	3.823	25.743	8.905 [‡]	18.224
C_{33}	7.422	20.344	2.390	6.943	-0.113	5.243	13.540	2.198	19.459	2.543 [‡]	9.234
K_I	41.001	49.217	24.957	35.010	21.671	25.120	44.941	20.242	38.398	25.982	54.917
K_{II}	14.845	40.687	4.779	13.886	-0.227	10.485	27.080	14.407	5.475	8.329	18.469
K_{III}	14.845	40.687	4.779	13.886	-0.226	10.485	27.080	4.395	38.919	5.085	18.469
MAPE _{HD}		63.015	34.079	10.019	50.892	21.219	31.097	39.033	55.026	30.125	20.920

[†] Potential does not reproduce the correct symmetry of the structure ($a=b$),

[‡] Potential does not reproduce the isotropy of the elasticity tensor ($C_{11} \neq C_{22}$ and $2 \cdot C_{33} \neq C_{11} - C_{12}$),

* Negative Kelvin moduli K_i indicating a lack of mechanical stability.

TABLE VIII. Structural and mechanical properties of large honeycomb dumbbell (LHD) stanene from molecular calculations: lattice parameters a, b (\AA), average cohesive energy E_c (eV/atom), average bond length d (\AA), average height h (\AA), 2D elastic constants C_{ij} (N/m), 2D Kelvin moduli K_i (N/m), mean absolute percentage error (MAPE) (%), relative performance measured as normalized timesteps/second in molecular dynamics (MD) simulation.

Method	DFT	Tersoff 2016	MEAM 1997	MEAM 2017	MEAM 2018a	MEAM 2018b	RANN 2023	DP-PBE 2023	DP-SCAN 2023	POLY 2023	MTP 2024
a	8.890	9.175	9.090	8.788	8.977	8.907	9.467	9.103	8.220	9.017	8.724 [†]
b	8.890	9.175	9.090	8.788	8.977	8.907	9.467	9.103	8.220	9.017	8.821 [†]
$-E_c$	3.062	3.128	2.459	2.548	2.322	2.830	2.792	3.399	2.981	2.771	1762.220 [*]
d	2.897	3.037	3.046	2.938	3.130	2.894	7.508	2.968	3.066	2.922	1.570
h	3.404	3.976	4.153	3.968	4.853	3.617	2.932	3.492	5.058	3.638	2.515
C_{11}	33.028	62.603	21.657	28.337	23.896	16.664	23.408 [‡]	22.768	148.381 [‡]	7.968 [‡]	7739.930 [*]
C_{22}	33.028	62.603	21.657	28.337	23.896	16.664	22.444 [‡]	22.768	139.851 [‡]	9.575 [‡]	9143.533 [*]
C_{12}	15.753	25.854	10.222	11.978	7.496	7.277	18.709 [‡]	14.050	106.473 [‡]	15.109 [‡]	4278.919 [*]
C_{33}	8.637	18.374	5.718	8.180	8.200	4.693	1.940 [‡]	4.359	16.008 [‡]	-1.213 [‡]	2009.998 [*]
K_I	48.782	88.457	31.878	40.315	31.393	23.941	41.630	36.818	250.503	23.859	12662.705
K_{II}	17.275	36.748	11.435	16.360	16.400	9.387	4.223	8.718	37.729	-6.315	4220.75 [‡]
K_{III}	17.275	36.748	11.435	16.360	16.400	9.387	3.879	8.718	32.016	-2.427	4019.99 [‡]
MAPE _{LHD}		57.744	24.280	10.221	19.605	29.589	43.341	22.240	168.606	48.901	19337.268
MAPE		681.081	370.206	312.082	437.462	264.400	433.696	329.928	1503.894	668.989	19733.899
timesteps/s		4989.047	2159.590	4552.066	1980.937	5539.323	96.654	1.000	5.987	6.232	105.317

[†] Potential does not reproduce the correct symmetry of the structure ($a \neq b$),

[‡] Potential does not reproduce the isotropy of the elasticity tensor ($C_{11} \neq C_{22}$ and $2 \cdot C_{33} \neq$

$C_{11} - C_{12}$),

^{*} Negative Kelvin moduli K_i indicating a lack of mechanical stability,

• Highly overstated value.

IV. CONCLUSIONS

In the paper, a systematic quantitative comparison of different interatomic potentials of tin was carried out to reproduce the properties of seven allotropes of stanene (2D tin). In order to facilitate a comparative analysis of the ten interatomic potentials listed in Section II B, the structural and mechanical properties of the flat (F), low-buckled (LB), high-buckled (HB), full dumbbell (FD), trigonal dumbbell (TD), honeycomb dumbbell (HD) and large honeycomb dumbbell (LHD) (Figs. 1a)-g)) obtained by means of density functional theory (DFT) and molecular statics (MS) computations were used. Additionally, the computational cost and performance of the tested potentials were benchmarked.

- Only the Tersoff2016, MEAM1997 and MEAM2018b potentials correctly reconstruct the symmetry of crystals and their physical properties, see Tables II-VIII;
- The MEAM2018b potential ensures the best quantitative performance as measured by the total mean absolute percentage error (MAPE), see Table VIII;
- All five machine-learning-based potentials do not perform well in describing the mechanical properties of the seven polymorphs of stanene;
- The machine-learning-based interatomic potentials, when evaluated according to the methodology employed, are not demonstrably superior in performance (MAPE) to classical potentials. In fact, they are three orders of magnitude more computationally expensive, as evidenced Table VIII;
- In consideration of the performance, accuracy, and cost of computation, the classical potentials of the MEAM type appear to be the optimal choice in this context. Despite the absence of data for different polymorphs of stanene in the optimization of these potentials, they demonstrated the ability to reproduce their properties accurately. This is a consequence of their foundation in physical principles, their capacity for natural extrapolation, and their avoidance of mere interpolation.

The results obtained here confirm the previous observations^{7,8,17} that the machine-learning-based interatomic potentials, in accordance with the methodology applied, are not superior to classical potentials in terms of their accuracy/performance (MAPE) and are meanwhile up to orders of magnitude more computationally expensive, see Table VIII. In general, classical, physics-based potentials demonstrate better universality/transferability than purely interpolative potentials based on machine learning.

It is my hope that the findings presented here will prove useful to other researchers in the selection of suitable potentials for their purposes, as well as in the parametrization of new potentials for monolayer structures.

V. SUPPLEMENTARY MATERIAL

Crystallographic Information Files (CIFs) for polymorphs of stanene (created by qAgate: Open-source software to post-process ABINIT) are available online at Supplementary material.

- flat (F) stanene:

```
# Sn_F 'P6/MMM' 191 hexagonal
data_Sn
_symmetry_space_group_name_H-M   'P 1'
_cell_length_a   4.75336890
_cell_length_b   4.75336890
_cell_length_c   20.00000009
_cell_angle_alpha 90.00000000
_cell_angle_beta  90.00000000
_cell_angle_gamma 120.00000000
_symmetry_Int_Tables_number 1
_chemical_formula_structural Sn
_chemical_formula_sum   Sn2
_cell_volume   391.34849752
_cell_formula_units_Z   2
loop_
_symmetry_equiv_pos_site_id
_symmetry_equiv_pos_as_xyz
1 'x, y, z'
loop_
_atom_site_type_symbol
_atom_site_label
_atom_site_symmetry_multiplicity
_atom_site_fract_x
_atom_site_fract_y
_atom_site_fract_z
_atom_site_occupancy
Sn Sn0 1 0.33333333 0.66666667 0.50000000 1
Sn Sn1 1 0.66666667 0.33333333 0.50000000 1
```

- low-buckled (LB) stanene:

```
# SN_LB 'P-3M1' 164 trigonal
data_Sn
_symmetry_space_group_name_H-M   'P 1'
_cell_length_a   4.59395779
_cell_length_b   4.59395779
_cell_length_c   20.00000009
_cell_angle_alpha 90.00000000
_cell_angle_beta  90.00000000
_cell_angle_gamma 120.00000000
_symmetry_Int_Tables_number 1
_chemical_formula_structural Sn
_chemical_formula_sum   Sn2
_cell_volume   365.53976596
_cell_formula_units_Z   2
loop_
_symmetry_equiv_pos_site_id
_symmetry_equiv_pos_as_xyz
1 'x, y, z'
```

```

loop_
  _atom_site_type_symbol
  _atom_site_label
  _atom_site_symmetry_multiplicity
  _atom_site_fract_x
  _atom_site_fract_y
  _atom_site_fract_z
  _atom_site_occupancy
  Sn Sn0 1 0.33333333 0.66666667 0.47812944 1
  Sn Sn1 1 0.66666667 0.33333333 0.52187056 1

```

- high-buckled (HB) stanene:

```

# Sn_HB 'P-3M1' 164 trigonal
data_Sn
  _symmetry_space_group_name_H-M 'P 1'
  _cell_length_a 3.32896256
  _cell_length_b 3.32896256
  _cell_length_c 20.00000009
  _cell_angle_alpha 90.00000000
  _cell_angle_beta 90.00000000
  _cell_angle_gamma 120.00000000
  _symmetry_Int_Tables_number 1
  _chemical_formula_structural Sn
  _chemical_formula_sum Sn2
  _cell_volume 191.94572759
  _cell_formula_units_Z 2
loop_
  _symmetry_equiv_pos_site_id
  _symmetry_equiv_pos_as_xyz
  1 'x, y, z'
loop_
  _atom_site_type_symbol
  _atom_site_label
  _atom_site_symmetry_multiplicity
  _atom_site_fract_x
  _atom_site_fract_y
  _atom_site_fract_z
  _atom_site_occupancy
  Sn Sn0 1 0.33333333 0.66666667 0.56241445 1
  Sn Sn1 1 0.66666667 0.33333333 0.43758555 1

```

- full dumbbell (FD) stanene:

```

# Sn_FD 'P-6m2' 187 hexagonal
data_Sn
  _symmetry_space_group_name_H-M 'P 1'
  _cell_length_a 4.30887239
  _cell_length_b 4.30887239
  _cell_length_c 20.00000009
  _cell_angle_alpha 90.00000000
  _cell_angle_beta 90.00000000
  _cell_angle_gamma 120.00000000
  _symmetry_Int_Tables_number 1
  _chemical_formula_structural Sn
  _chemical_formula_sum Sn3

```

```

_cell_volume 321.57915851
_cell_formula_units_Z 3
loop_
_symmetry_equiv_pos_site_id
_symmetry_equiv_pos_as_xyz
1 'x, y, z'
loop_
_atom_site_type_symbol
_atom_site_label
_atom_site_symmetry_multiplicity
_atom_site_fract_x
_atom_site_fract_y
_atom_site_fract_z
_atom_site_occupancy
Sn Sn0 1 0.33333333 0.66666667 0.41833575 1
Sn Sn1 1 0.66666667 0.33333333 0.50000000 1
Sn Sn2 1 0.33333333 0.66666667 0.58166425 1

```

- trigonal dumbbell (TD) stanene:

```

# Sn_P3xP3td 'P-62M' 189 hexagonal
data_Sn
_symmetry_space_group_name_H-M 'P 1'
_cell_length_a 7.82139920
_cell_length_b 7.82139920
_cell_length_c 20.00000009
_cell_angle_alpha 90.00000000
_cell_angle_beta 90.00000000
_cell_angle_gamma 120.00000000
_symmetry_Int_Tables_number 1
_chemical_formula_structural Sn
_chemical_formula_sum Sn7
_cell_volume 1059.56971067
_cell_formula_units_Z 7
loop_
_symmetry_equiv_pos_site_id
_symmetry_equiv_pos_as_xyz
1 'x, y, z'
loop_
_atom_site_type_symbol
_atom_site_label
_atom_site_symmetry_multiplicity
_atom_site_fract_x
_atom_site_fract_y
_atom_site_fract_z
_atom_site_occupancy
Sn Sn0 1 -0.00000000 0.00000000 0.50000000 1
Sn Sn1 1 -0.03884085 0.33333333 0.50000000 1
Sn Sn2 1 0.37217418 0.03884085 0.50000000 1
Sn Sn3 1 0.66666667 0.33333333 0.41216092 1
Sn Sn4 1 0.33333333 0.66666667 0.50000000 1
Sn Sn5 1 0.66666667 0.62782582 0.50000000 1
Sn Sn6 1 0.66666667 0.33333333 0.58783908 1

```

- honeycomb dumbbell (HD) stanene:

```

# Sn_P3xP3hd 'P-62M' 189 hexagonal
data_Sn
_symmetry_space_group_name_H-M   'P 1'
_cell_length_a    7.64601637
_cell_length_b    7.64601637
_cell_length_c    20.00000009
_cell_angle_alpha 90.00000000
_cell_angle_beta  90.00000000
_cell_angle_gamma 120.00021772
_symmetry_Int_Tables_number 1
_chemical_formula_structural Sn
_chemical_formula_sum   Sn8
_cell_volume    1012.58181347
_cell_formula_units_Z   8
loop_
_symmetry_equiv_pos_site_id
_symmetry_equiv_pos_as_xyz
  1 'x, y, z'
loop_
_atom_site_type_symbol
_atom_site_label
_atom_site_symmetry_multiplicity
_atom_site_fract_x
_atom_site_fract_y
_atom_site_fract_z
_atom_site_occupancy
Sn Sn0 1 -0.00000831 -0.00000831 0.50000000 1
Sn Sn1 1 -0.00000211 0.36326058 0.50000000 1
Sn Sn2 1 0.36326058 -0.00000211 0.50000000 1
Sn Sn3 1 0.66666178 0.33332813 0.41774698 1
Sn Sn4 1 0.33332813 0.66666178 0.41774698 1
Sn Sn5 1 0.63674001 0.63674001 0.50000000 1
Sn Sn6 1 0.66666178 0.33332813 0.58225302 1
Sn Sn7 1 0.33332813 0.66666178 0.58225302 1

```

- large honeycomb dumbbell (LHD) stanene:

```

# Sn_P3xP3lhd 'P6/MMM' 191 hexagonal
data_Sn
_symmetry_space_group_name_H-M   'P 1'
_cell_length_a    8.89033525
_cell_length_b    8.89033525
_cell_length_c    20.00000009
_cell_angle_alpha 90.00000000
_cell_angle_beta  90.00000000
_cell_angle_gamma 120.00000000
_symmetry_Int_Tables_number 1
_chemical_formula_structural Sn
_chemical_formula_sum   Sn10
_cell_volume    1368.97937660
_cell_formula_units_Z   10
loop_
_symmetry_equiv_pos_site_id
_symmetry_equiv_pos_as_xyz
  1 'x, y, z'
loop_

```

<u>_atom_site_type_symbol</u>							
<u>_atom_site_label</u>							
<u>_atom_site_symmetry_multiplicity</u>							
<u>_atom_site_fract_x</u>							
<u>_atom_site_fract_y</u>							
<u>_atom_site_fract_z</u>							
<u>_atom_site_occupancy</u>							
Sn	Sn0	1	0.18240377	0.36480755	0.50000000	1	
Sn	Sn1	1	0.36480755	0.18240377	0.50000000	1	
Sn	Sn2	1	0.18240377	0.81759623	0.50000000	1	
Sn	Sn3	1	0.33333333	0.66666667	0.41489168	1	
Sn	Sn4	1	0.66666667	0.33333333	0.41489168	1	
Sn	Sn5	1	0.81759623	0.18240377	0.50000000	1	
Sn	Sn6	1	0.63519245	0.81759623	0.50000000	1	
Sn	Sn7	1	0.81759623	0.63519245	0.50000000	1	
Sn	Sn8	1	0.33333333	0.66666667	0.58510832	1	
Sn	Sn9	1	0.66666667	0.33333333	0.58510832	1	

ACKNOWLEDGMENTS

This work was supported by the National Science Centre (NCN – Poland) Research Project: No. 2021/43/B/ST8/03207. The computational assistance was granted through the computing cluster GRAFEN at Biocentrum Ochota, the Interdisciplinary Centre for Mathematical and Computational Modelling of Warsaw University (ICM UW) and Poznań Supercomputing and Networking Center (PSNC).

AUTHOR DECLARATION

Conflict of Interest

The author declare that they have no known competing financial interests or personal relationships that could have appeared to influence the work reported in this paper.

REFERENCES

- ¹K. S. Novoselov, A. K. Geim, S. V. Morozov, D. Jiang, Y. Zhang, S. V. Dubonos, I. V. Grigorieva, and A. A. Firsov, “Electric Field Effect in Atomically Thin Carbon Films,” *Science* 306, 666–669 (2004).
- ²J. Yuhara and G. L. Lay, “Beyond silicene: synthesis of germanene, stanene and plumbene,” *Japanese Journal of Applied Physics* 59, SN0801 (2020).
- ³M. W. Ochapski and M. P. de Jong, “Progress in epitaxial growth of stanene,” *Open Physics* 20, 208–223 (2022).
- ⁴J. Yuhara, Y. Fujii, K. Nishino, N. Isobe, M. Nakatake, L. Xian, A. Rubio, and G. L. Lay, “Large area planar stanene epitaxially grown on Ag(1 1 1),” *2D Materials* 5, 025002 (2018).
- ⁵J.-K. Lyu, S.-F. Zhang, C.-W. Zhang, and P.-J. Wang, “Stanene: A Promising Material for New Electronic and Spintronic Applications,” *Annalen der Physik* 531, 1900017 (2019).
- ⁶F. Matusalem, M. Marques, L. K. Teles, and F. Bechstedt, “Stability and electronic structure of two-dimensional allotropes of group-IV materials,” *Phys. Rev. B* 92, 045436 (2015).
- ⁷M. Ma´zdziaż, “Transferability of interatomic potentials for silicene,” *Beilstein Journal of Nanotechnology* 14, 574–585 (2023).
- ⁸M. Ma´zdziaż, “Transferability of interatomic potentials for germanene (2D germanium),” *Journal of Applied Physics* 134, 184303 (2023).
- ⁹P. Tang, P. Chen, W. Cao, H. Huang, S. Cahangirov, L. Xian, Y. Xu, S.-C. Zhang, W. Duan, and A. Rubio, “Stable two-dimensional dumbbell stanene: A quantum spin Hall insulator,” *Phys. Rev. B* 90, 121408 (2014).

- ¹⁰P. Rivero, J.-A. Yan, V. M. García-Suárez, J. Ferrer, and S. Barraza-Lopez, “Stability and properties of high-buckled two-dimensional tin and lead,” *Phys. Rev. B* 90, 241408 (2014).
- ¹¹S. Cahangirov, V. O. Ozcelik, L. Xian, J. Avila, S. Cho, M. C. Asensio, S. Ciraci, and A. Rubio, “Atomic structure of the $\sqrt{3} \times \sqrt{3}$ phase of silicene on Ag(111),” *Phys. Rev. B* 90, 035448 (2014).
- ¹²B. van den Broek, M. Houssa, E. Scalise, G. Pourtois, V. V. Afanas’ev, and A. Stesmans, “Two-dimensional hexagonal tin: *ab initio* geometry, stability, electronic structure and functionalization,” *2D Materials* 1, 021004 (2014).
- ¹³R. John and B. Merlin, “Theoretical Investigation of Structural, Electronic, and Mechanical Properties of Two Dimensional C, Si, Ge, Sn,” *Crystal Structure Theory and Applications* 5, 43–55 (2016).
- ¹⁴L. Tao, C. Yang, L. Wu, L. Han, Y. Song, S. Wang, and P. Lu, “Tension-induced mechanical properties of stanene,” *Modern Physics Letters B* 30, 1650146 (2016).
- ¹⁵A. K. A. Kandy, K. Rossi, A. Raulin-Foissac, G. Laurens, and J. Lam, “Comparing transferability in neural network approaches and linear models for machine-learning interaction potentials,” *Phys. Rev. B* 107, 174106 (2023).
- ¹⁶C. de Tomas, A. Aghajamali, J. L. Jones, D. J. Lim, M. J. López, I. Suarez-Martinez, and N. A. Marks, “Transferability in interatomic potentials for carbon,” *Carbon* 155, 624–634 (2019).
- ¹⁷M. Maździarz, “Transferability of Molecular Potentials for 2D Molybdenum Disulphide,” *Materials* 14 (2021), 10.3390/ma14030519.
- ¹⁸P. Hohenberg and W. Kohn, “Inhomogeneous electron gas,” *Phys. Rev.* 136, B864–B871 (1964).
- ¹⁹W. Kohn and L. J. Sham, “Self-consistent equations including exchange and correlation effects,” *Phys. Rev.* 140, A1133–A1138 (1965).
- ²⁰D. R. Hamann, X. Wu, K. M. Rabe, and D. Vanderbilt, “Metric tensor formulation of strain in density-functional perturbation theory,” *Phys. Rev. B* 71, 035117 (2005).
- ²¹X. Gonze, B. Amadon, G. Antonius, F. Arnardi, L. Baguet, J.-M. Beuken, J. Bieder, F. Bottin, J. Bouchet, E. Bousquet, N. Brouwer, F. Bruneval, G. Brunin, T. Cavignac, J.-B. Charraud, W. Chen, M. Coˆtˆe, S. Cottenier, J. Denier, G. Geneste, P. Ghosez, M. Giantomassi, Y. Gillet, O. Gingras, D. R. Hamann, G. Hautier, X. He, N. Helbig, N. Holzwarth, Y. Jia, F. Jollet, W. Lafargue-Dit-Hauret, K. Lejaeghere, M. A. Marques, A. Martin, C. Martins, H. P. Miranda, F. Naccarato, K. Persson, G. Petretto, V. Planes, Y. Pouillon, S. Prokhorenko, F. Ricci, G.-M. Rignanese, A. H. Romero, M. M. Schmitt, M. Torrent, M. J. van Setten, B. V. Troeye, M. J. Verstraete, G. Zˆerah, and J. W. Zwanziger, “The ABINIT project: Impact, environment and recent developments,” *Computer Physics Communications* 248, 107042 (2020).
- ²²J. P. Perdew, A. Ruzsinszky, G. I. Csonka, O. A. Vydrov, G. E. Scuseria, L. A. Constantin, X. Zhou, and K. Burke, “Restoring the Density-Gradient Expansion for Exchange in Solids and Surfaces,” *Phys. Rev. Lett.* 100, 136406 (2008).
- ²³D. R. Hamann, “Optimized norm-conserving Vanderbilt pseudopotentials,” *Phys. Rev. B* 88, 085117 (2013).
- ²⁴M. van Setten, M. Giantomassi, E. Bousquet, M. Verstraete, D. Hamann, X. Gonze, and G.-M. Rignanese, “The PseudoDojo: Training and grading a 85 element optimized norm-conserving pseudopotential table,” *Computer Physics Communications* 226, 39–54 (2018).
- ²⁵S. Plimpton, “Fast Parallel Algorithms for Short-Range Molecular Dynamics,” *Journal of Computational Physics* 117, 1 – 19 (1995).
- ²⁶A. Stukowski, “Visualization and analysis of atomistic simulation data with OVITO - the Open Visualization Tool (<http://ovito.org/>),” *Modelling Simul. Mater. Sci. Eng.* 18, 015012 (2010).
- ²⁷“NIST Interatomic Potentials Repository: <http://www.ctcms.nist.gov/potentials/>,”.
- ²⁸M. J. Cherukara, B. Narayanan, A. Kinaci, K. Sasikumar, S. K. Gray, M. K. Chan, and S. K. R. S. Sankaranarayanan, “*Ab Initio*-Based Bond Order Potential to Investigate Low Thermal Conductivity of Stanene Nanostructures,” *The Journal of Physical Chemistry Letters* 7, 3752–3759 (2016).
- ²⁹R. Ravelo and M. Baskes, “Equilibrium and Thermodynamic Properties of Grey, White, and Liquid Tin,” *Phys. Rev. Lett.* 79, 2482–2485 (1997).
- ³⁰J. Vella, M. Chen, F. H. Stillinger, E. A. Carter, P. G. Debenedetti, and A. Z. Panagiotopoulos, “Structural and dynamic properties of liquid tin from a new modified embedded-atom method force field,” *Phys. Rev. B* 95, 064202 (2017).
- ³¹S. A. Etesami, M. I. Baskes, M. Laradji, and E. Asadi, “Thermodynamics of solid Sn and Pb-Sn liquid mixtures using molecular dynamics simulations,” *Acta Materialia* 161, 320–330 (2018).
- ³²W.-S. Ko, D.-H. Kim, Y.-J. Kwon, and M. H. Lee, “Atomistic Simulations of Pure Tin Based on a New Modified Embedded-Atom Method Interatomic Potential,” *Metals* 8 (2018), 10.3390/met8110900.
- ³³M. S. Nitol, K. Dang, S. J. Fensin, M. I. Baskes, D. E. Dickel, and C. D. Barrett, “Hybrid interatomic potential for Sn,” *Phys. Rev. Mater.* 7, 043601 (2023).
- ³⁴T. Chen, F. Yuan, J. Liu, H. Geng, L. Zhang, H. Wang, and M. Chen, “Modeling the high-pressure solid and liquid phases of tin from deep potentials with *ab initio* accuracy,” *Phys. Rev. Mater.* 7, 053603 (2023).
- ³⁵J. Zeng, D. Zhang, D. Lu, P. Mo, Z. Li, Y. Chen, M. Rynik, L. Huang, Z. Li, S. Shi, Y. Wang, H. Ye, P. Tuo, J. Yang, Y. Ding, Y. Li, D. Tisi, Q. Zeng, H. Bao, Y. Xia, J. Huang, K. Muraoka, Y. Wang, J. Chang, F. Yuan, S. L. Bore, C. Cai, Y. Lin, B. Wang, J. Xu, J.-X. Zhu, C. Luo, Y. Zhang, R. E. A. Goodall, W. Liang, A. K. Singh, S. Yao, J. Zhang, R. Wentzcovitch, J. Han, J. Liu, W. Jia, D. M. York, W. E. R. Car, L. Zhang, and H. Wang, “DeePMD-kit v2: A software package for deep potential models,” *The Journal of Chemical Physics* 159, 054801 (2023).

- ³⁶J. P. Perdew, K. Burke, and M. Ernzerhof, “Generalized Gradient Approximation Made Simple,” *Phys. Rev. Lett.* 77, 3865–3868 (1996).
- ³⁷J. Sun, A. Ruzsinszky, and J. P. Perdew, “Strongly Constrained and Appropriately Normed Semilocal Density Functional,” *Phys. Rev. Lett.* 115, 036402 (2015).
- ³⁸A. Seko, “Tutorial: Systematic development of polynomial machine learning potentials for elemental and alloy systems,” *Journal of Applied Physics* 133, 011101 (2023).
- ³⁹H. Mei, L. Chen, F. Wang, G. Liu, J. Hu, W. Lin, Y. Shen, J. Li, and L. Kong, “Development of machine learning and empirical interatomic potentials for the binary Zr-Sn system,” *Journal of Nuclear Materials* 588, 154794 (2024).
- ⁴⁰I. S. Novikov, K. Gubaev, E. V. Podryabinkin, and A. V. Shapeev, “The MLIP package: moment tensor potentials with MPI and active learning,” *Machine Learning: Science and Technology* 2, 025002 (2020).
- ⁴¹M. Maździarz, “Comment on ‘The Computational 2D Materials Database: high-throughput modeling and discovery of atomically thin crystals’,” *2D Materials* 6, 048001 (2019).
- ⁴²J. Nye and P. Nye, *Physical Properties of Crystals: Their Representation by Tensors and Matrices*, Oxford science publications (Clarendon Press, 1985).
- ⁴³M. Maździarz and M. Gajewski, “Estimation of Isotropic Hyperelasticity Constitutive Models to Approximate the Atomistic Simulation Data for Aluminium and Tungsten Monocrystals,” *Computer Modeling in Engineering & Sciences* 105, 123–150 (2015).
- ⁴⁴A. M. Miksch, T. Morawietz, J. K“astner, A. Urban, and N. Artrith, “Strategies for the construction of machine-learning potentials for accurate and efficient atomic-scale simulations,” *Machine Learning: Science and Technology* 2, 031001 (2021).